Periodico di Mineralogia (2014), 83, 3, 401-418 DOI: 10.2451/2014PM0022

PERIODICO di MINERALOGIA
established in 1930

An International Journal of
MINERALOGY, CRYSTALLOGRAPHY, GEOCHEMISTRY,
ORE DEPOSITS, PETROLOGY, VOLCANOLOGY
and applied topics on Environment, Archaeometry and Cultural Heritage

Crystallization from a melt and crystallization at subsolidus conditions: comparison from crystal size distribution study on Gennargentu Rocks (Sardinia, Italy)

Valeria Misiti[1,*], Francesco Vetere[2] and Florian Heidelbach[3]

[1]Istituto Nazionale di Geofisica e Vulcanologia, Sezione di Sismologia e Tettonofisica
Via di Vigna Murata 605, I-00143 Rome Italy,
[2]Università degli Studi di Perugia, Dipartimento di Fisica e Geologia,
Piazza dell'Università 1, I-06123 Perugia, Italy
[3]Bayerisches Geoinstitut, Universität Bayreuth, Universitätstraβe 30, D-95447 Bayreuth, Germany
[*]Corresponding author: *valeria.misiti@ingv.it*

Abstract

Plagioclase crystal size distribution (CSD) has been investigated in a quartz-diorite body, in the leucosome of migmatites and in the melanosome of un-melted contact metamorphic rocks from Gennargentu Complex (Sardinia, Italy). During the crystallization of the dioritic magma, a variety of competing kinetic processes determine the evolution of the igneous microstructure, but the relative contribution of each process remains elusive. Our approach was aimed to study the plagioclase crystallization from a liquid (quartz-diorites and migmatite leucosomes), comparing it to a crystallization at subsolidus conditions. CSD indicates that plagioclase in the quartz-diorite nucleated and grew in a cooling system at a constant cooling rate, producing straight-line CSD in a diagram of ln of population density vs. size range. The plagioclase crystallization continued until the latent heat was available and the temperature was high enough to allow the plagioclase growing. This can occur only when a crystal is held at temperature close to its liquidus for a long period of time. Under these conditions, the plagioclase nucleation rate is zero, but growth rate is high for crystal larger than the critical size. This does not necessarily mean that the temperature was held constant, just that the undercooling remained small (Ostwald ripening process). The aggregated small crystals, due to their high surface energy per unit volume, to minimise energy in the system dissolved and

"fed" the growth of larger crystals. This process occurs because small grains have a higher surface energy per unit volume than do larger grains. The crystallization temperature (~900 °C, 100 MPa) allows the formation of plagioclase as liquidus phase. From CSD measurements we calculated the different cooling ages for the different sample types.

Key words: Crystal size distributions; Gennargentu Igneous Complex; plagioclase; subsolidus crystallization; Ostwald ripening.

Introduction

The heat released by the emplacement of a plutonic body has been identified as the major responsible for contact metamorphic aureole formation and even migmatization (i.e., partial melting; Brown et al., 1995). The texture of an igneous rock is a fundamental source of information to infer the physical conditions under which the rock crystallized. The number, size and shape of the crystals present in an igneous rock reflect the nucleation and growth rates and the degree of departure from chemical equilibrium during its cooling history.

To date, the application of crystal size distribution (CSD) to natural samples has generally been limited to qualitative studies of magmatic crystallization processes (estimates of relative cooling rates, Garrido et al., 2001; crystal settling and compaction, Higgins, 2002; Bindeman 2003). Zieg and Marsh (2002), Conte et al. (2006), Armienti et al. (2007) and Resmini (2007) have presented successful quantitative physical models for natural and synthetic CSD in magmatic bodies. Up to now, most of the studies employing CSD have been focused on volcanic rocks (i.e., Marsh, 1998), whereas studies on intrusive (Higgins, 1998, 1999) and metamorphic rocks (Covey-Crump and Rutter, 1989; Berger and Roselle, 2001) have received much less attention in this respect. Coarsening in a melt system results in a different CSD trend compared to a constant crystal growth process. The coarsening in a subsolidus (metamorphic) system results in a normal CSD pattern (Nam et al., 1999).

The CSD analysis performed here aims to evidence the differences between the crystallization from a melt (quartz-diorite and leucosome) and that from a solid (contact metamorphic rock). In this regard, a CSD study has been carried out on selected samples belonging to the Gennargentu Complex (Sardinia, Italy) to clarify the crystallization processes from a liquid acting in the quartz-diorite and migmatite leucosome as well as the subsolidus processes acting in the contact metamorphosed basement. The Gennargentu Igneous Complex is one of the best examples of a contact aureole generated at low-P and high-T (100 MPa, 780-820 °C), where the temperature of the plutonic body (quartz-diorite) was high enough to cause partial melting of the metapelitic rocks in the contact aureole (Misiti et al., 2005).

The Gennargentu Complex

Geological setting

The Gennargentu Igneous Complex (hereafter GIC) is situated in the southern flank of Gennargentu Mountains in central-eastern Sardinia and is exposed over an area of approximately 30 km^2.

The complex was emplaced into greenschist-facies metapelitic rocks of the Nappe Zone of the Variscan chain (Franceschelli et al., 1992). The Nappe Zone constitutes the central part of Sardinia and originates from the early Carboniferous Variscan collision (Carmignani et al., 1994) between the postulated supercontinents of Gondwana and Laurasia (or Armorica) or at least between minor segments of them (Vai and Cocozza, 1986). The post-collisional evolution of Variscan chain of Sardinia was characterised by a regional strike-slip phase that favoured the emplacement of the Sardinian-Corsican Batholith (SCB; Carosi et al., 2012; Casini et al., 2012; Padovano et al., 2014). The SCB is a heterogeneous assortment of intrusive rocks ranging from monzogranites and granodiorites, which constitute more than 65% of the outcrops, to rare gabbros and felsic differentiated rocks such as leucogranites (Poli et al., 1989). The GIC is a small part of the SCB and is composed of different types of Carboniferous peraluminous granite, a late Permian quartz-diorite intrusion and volcanic rocks (Figure 1).

The GIC contains two main intrusive units 1) peraluminous granites (two-mica granodiorites grading to muscovite leucogranites with andalusite and garnet, and 2) quartz-diorites (Figure 1). Gaeta et al. (2000; 2013) have subdivided the GIC peraluminous granites into three genetically related groups: 1) two-mica monzogranites and granodiorites; 2) two-mica, alkali feldspar-rich leucogranites with andalusite and garnet; 3) fine-grained muscovite-bearing leucogranites intruded as dykes.

The quartz-diorite intrusion crops out in the western part of the GIC with a surface of 6 km^2 and shows local variations in colour, mineralogy and chemical composition (Cozzupoli et al., 1995). In particular, it shows two coarse-grained facies ranging in colour from dark to grey and a poor, dark fine-grained facies, occurring as syn-plutonic dikes. Peraluminous granites were intruded in the north western sector by quartz-diorite body. The P range under which peraluminous granites crystallized has been inferred by microthermometric data combined with chemical-petrographic characteristics suggesting that peraluminous granites crystallized under a P of 300-400 MPa (Gaeta et al., 2000). Thermobarometric calculations and phase equilibria experiments indicate that the H_2O-undersaturated quartz-diorite magma was emplaced at pressure of 100 MPa and temperature of ~900 °C. The quartz-diorite intrusion developed a thick (~500 m) thermometamorphic aureole with a mineralogy that varies depending on the protolith composition (metapelitic or granitic) and peak temperature (Cozzupoli et al., 1997). This indicates that Gennargentu Igneous Complex is a polybaric body. The only available data, even if poorly constrained and old (Cozzupoli et al., 1997; Misiti, 2004; Misiti et al., 2005) reported

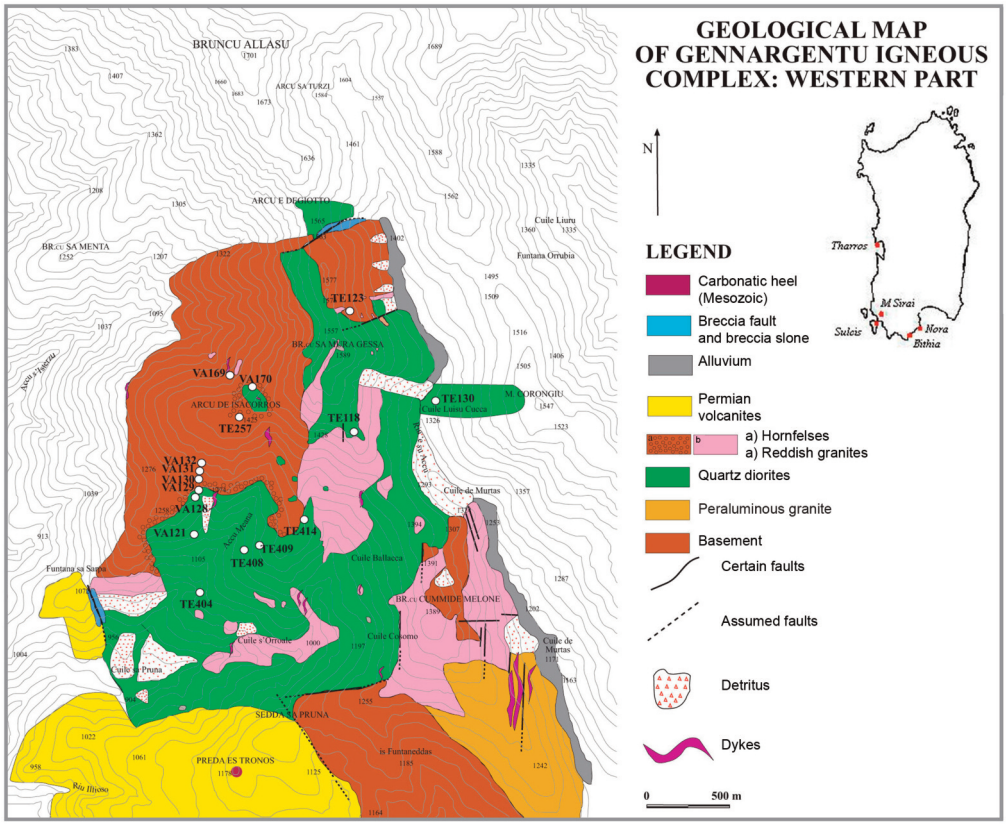

Figure 1. Geological map of Gennargentu Igneous Complex: Western part.

bulk rock Rb/Sr ages of 310 ± 6 Ma for the peraluminous granites and 253 ± 3 Ma for the quartz-diorite intrusion. The age of the quartz-diorite overlaps with the age of the volcanic activity occurred in the Gennargentu area (Cozzupoli et al., 1971; Edel et al., 1981). A well exposed contact metamorphic aureole, whose thickness vary from few meters to hundred of meters, fringes the entire intrusive complex. The regional greenschists become albite-epidote and biotite-plagioclase hornfels due to the emplacement of peraluminous granites with the formation of andalusite and tourmaline porphyroblasts (Cozzupoli et al., 1997).

The chemical composition of the GIC volcanic rocks ranges from high-K dacite to high-K rhyolite. The quartz-diorite intrusion crops out in the western part of the GIC with a surface area of ~6 km^2 and shows local variations in rock colour, mineralogy and chemical composition (Cozzupoli et al., 1995).

Field relationships and sampling

The GIC provides ideal conditions for fieldwork owing to the paucity of vegetation and abundance of outcrops. The contact between quartz-diorite and metapelites is well exposed and it is possible to observe the morphology and the main features on a macroscopic scale. The regionally-metamorphosed metapelitic rocks are the dominant wall rocks. They can be subdivided into three metamorphic zones that, in order of increasing grade toward the intrusion are: 1) cordierite-andalusite hornfels zone; 2) transition zone (hereafter contact aureole); 3) migmatite zone.

Particular attention has been focused on the study of the migmatite zone, which extends for approximately 50 m in direct contact with the quartz-dioritic body. Sampling in this study had the main objectives in documenting the petrography of the peripheral zone of quartz-diorite intrusion and in investigating the variation in the migmatite zone corresponding to the distance from the contact with quartz-diorite intrusion. We collected 16 samples among quartz-diorite and metapelitic rocks along a traverse from the quartz-diorite contact towards the migmatitic rocks (Figure 1).

Petrography and chemistry of collected samples

Quartz dioritic rocks

The dark quartz-diorites (Table 1) show isotropic and inequigranular texture. The main peculiar feature of these rocks is the granophyric texture which is present in all the samples as plumose and vermicular. In general, this texture is present along the plagioclase boundaries as interstice. The mineral assemblage consists of plagioclase, K-feldspar, biotite, amphibole, quartz and pyroxene; accessories are magnetite, hercynite, zircon and epidote.

Plagioclase is the most abundant phase, with a grain-size up to about 8 mm. It shows sericitic alteration in the cores and normal zoning from

Table 1. Chemical composition of quartz-diorite samples.

	Dark quartz diorite			Light quartz diorite				
SiO_2	59.66	54.83	56.81	59.84	58.2	53.96	58.06	55.61
TiO_2	0.83	0.96	0.973	0.15	0.92	1.58	0.862	0.99
Al_2O_3	16.58	18.38	17.82	17.31	16.12	12.29	17.59	17.46
Fe_2O_3	2.16	7.77	7.12	2.01	1.76	8.27	6.8	2.53
FeO	3.56	0,00	0,00	2.61	4.66	4.4	0,00	4.69
MnO	0.1	0.12	0.12	0.07	0.14	0.23	0.11	0.14
MgO	2.8	4.14	3.6	3.55	5.09	2.2	3.51	4.07
CaO	5.61	7.71	7.25	6.29	5.56	10.03	6.52	7.45
Na_2O	2.63	2.63	2.54	3.78	2.2	0.64	2.56	2.37
K_2O	2.66	1.05	1.54	1.42	2.49	4.07	1.97	1.81
P_2O_5	0.15	0.18	0.15	0.15	0.19	0.18	0.16	0.17
L.O.I.	2.33	1.85	1.59	1.63	2.66	2.15	1.85	2.2
Total	99.07	99.62	99.51	98.81	99.99	100.00	99.99	99.49

bytownite to albite. It contains inclusions of euhedral magnetite, amphibole and pyroxene; the smallest plagioclases are sodic (andesine).

Sub-millimetre K-feldspar and quartz are both anhedral and are sometimes intergrown to form microgranophyre. The interstices are occupied by poikilitic quartz with inclusions of plagioclase, biotite and Fe-Ti oxides (Figure 2). Amphibole is the most abundant mafic phase, followed by clinopyroxene. Amphibole crystals are 1 to 2 mm long, typically fibrous in texture, weakly pleochroic and have been identified as actinolite. Clinopyroxene is more abundant than orthopyroxene (Figure 2) and shows inclusions of Fe-Ti oxides and plagioclase that become more abundant toward the rims. Clinopyroxene crystals are subhedral to anhedral and 2 to 3 mm long. Orthopyroxene is only present either as inclusions in clinopyroxene or as relicts, partially pseudomorphed by actinolite.

There are significant modal variations among samples collected in the light quartz-diorite (Table 1) . The main variation concerns the modal abundance of K-feldspar. This shifts the rock compositions from the quartz-diorite field into granodiorite and quartz monzodiorite. The anhedral K-feldspar crystals are quite small ≤ 2 to 3 mm; powder X-ray diffraction analyses show that these feldspars are orthoclase to sanidine. The amphiboles are either actinolites or hornblendes, with the euhedral to subhedral hornblende included in quartz crystals.

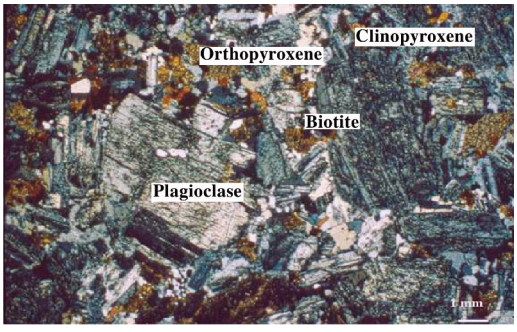

Figure 2. Sample VA128 reported in Figure 1. The dark quartz-diorite showing the presence of plagioclase, orthopyroxene, clinopyroxene and biotite crystals.

Contact aureole

The transition from quartz-diorite through thermometamorphic rocks to the migmatite zone can be easily identified on the basis of petrography. The migmatite samples have a widely spaced gradational foliation defined by alternating leucosome and melanosome layers. On the basis of petrographic, structural and textural features of the rocks, two groups of migmatites can be identified: a) migmatites s.s. and b) injected migmatites. A third type (hybrid rocks) comprises wall-rock xenoliths in the quartz-diorite. The chemical compositions of the three rock types are reported in Table 2.

Migmatites s.s.

These rocks show a folded foliation formed by the alternation of leucosome and melanosome layers. The leucosome consists of coarse-grained quartz and K-feldspar, commonly exhibiting granophyric intergrowths (Figure 3), with sparse large sub-euhedral chlorite crystals usually with oxide inclusions. Magnetites are accumulated at the edges of the leucosome layers, with a grain size reducing from ~5 mm at core to ~0.2 mm at

Table 2. Chemical composition of metamorphic rocks.

	Migmatite s.s.				Injected migmatites			Hybrid rocks	
SiO_2	59.08	53.73	50.22	54.68	56.63	62.53	55.26	46.21	52.52
TiO_2	0.78	0.93	1.87	1.02	1.17	0.77	1.21	1.36	1.02
Al_2O_3	17.00	21.32	16.5	18.26	16.47	13.54	18.43	26.45	22.25
Fe_2O_3	3.83	4.23	2.46	4.5	5.25	5.11	6.78	6.32	4.30
FeO	2.55	3.55	11.01	2.95	2.06	3.68	2.23	2.55	3.83
MnO	0.09	0.06	0.11	0.097	0.129	0.196	0.187	0.10	0.09
MgO	5.54	5.52	7.06	3.9	4.4	3.19	4.56	3.19	4.01
CaO	2.69	1.08	2.81	4.33	5.08	2.40	2.00	2.56	1.15
Na_2O	2.73	2.18	1.34	2.76	2.10	1.57	1.06	2.33	3.18
K_2O	2.41	2.95	1.08	1.78	2.38	1.78	2.7	4.87	5.52
P_2O_5	0.15	0.09	0.05	0.10	0.13	0.17	0.17	0.06	0.07
L.O.I.	3.19	4.35	4.33	4.41	3.05	4.33	4.12	3.57	2.03
Total	100.04	99.99	98.84	98.80	98.85	99.27	98.70	99.57	99.97

edge. The habit and peculiar distribution of magnetite, as well as the occurrence of granophyric structures, highlight the formation of leucosome from a melt (Figure 3).The granophyric development requires the presence of phenocryst hosts from which the skeletal crystals emanate. Low pressure aids their development: magma depth must be sufficiently shallow (3 km) so that pressure changes can cause enough H_2O loss to drive rapid undercooling. Melanosome layers are mainly composed of cordierite and plagioclase intergrowth. Cordierite crystals are unzoned, locally reach sub-millimeter size and are mostly associated with "clouds" of hercynite (Figure 4). Rare biotite crystals are characterised by rounded magnetite inclusions and show cuspate edges which are interstitial between cordierite and plagioclase. Relicts of andalusite, with pink portions (corresponding to a Fe-rich composition), occur as centimetre-sized porphyroblasts partially replaced by hercynite + cordierite or by corundum ± black spinel. Apatite tends to form mono-mineralic clusters. The abundance of dry high-T phases (i.e.,

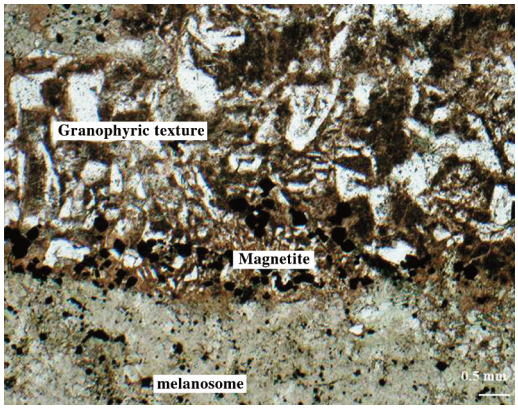

Figure 3. Sample TE257. These rocks show folded foliations formed by the alternation of leucosome and melanosome layers. The leucosome consists of coarse-grained quartz and K-feldspar, commonly exhibiting granophyric intergrowths, with sparse large sub-euhedral chlorite crystals usually with inclusions of rutile needles. Magnetites are accumulated at edges of leucosome layers.

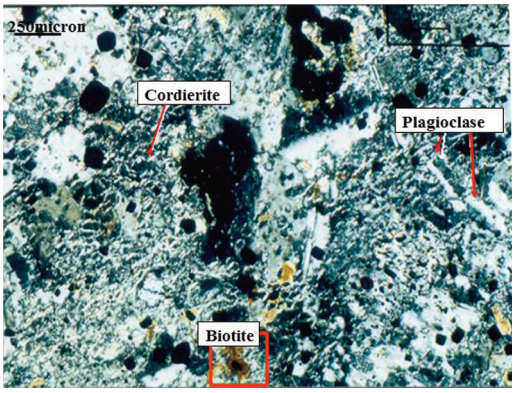

Figure 4. Melanosome layer. Pinitised cordierite with plagioclase, magnetite and trace of residual biotite with magnetite core (in the red square).

plagioclase, hercynite, cordierite, corundum) and the exclusive occurrence of blastic crystallization can be interpreted the melanosome as restitic layers resulting from the migmatization process.

Injected Migmatites (IM)

These rocks are foliated as the previous migmatites and it is possible to recognize two main layer types. Large grain-sized leucocratic layers are mainly formed by mesopertitic K-feldspar, quartz, and minor amount of plagioclase, biotite, and magnetite, while the melanocratic layers are composed of biotite, cordierite and pyroxene (Figure 5). Quartz occurs at least in four ways: 1) as sub-rounded relicts in K-feldspar; 2) in graphic structure with plagioclase; 3) in interstitial pockets surrounded by plagioclase; 4) polygonal aggregates. Plagioclase shows a very interesting texture: it is frequently rooted in the layer boundaries and grows perpendicular to the foliation with an elongated euhedral habit.

Fine-grained melanocratic layers are mainly characterized by cordierite (often pinitised), plagioclase, decussated biotite, hercynite and corundum swarms and tourmaline. Quartz, andalusite, rutile and ilmenite are sporadic. These layers preserve a weak foliation, due to biotite and corundum swarms, evidently inherited by the protolith. The boundaries of leucocratic layers are often characterized by biotite concentrations and the melanocratic layers are interlocked with lenticular medium- to fine-grained domains formed by a quartz-feldspatic granoblastic texture.

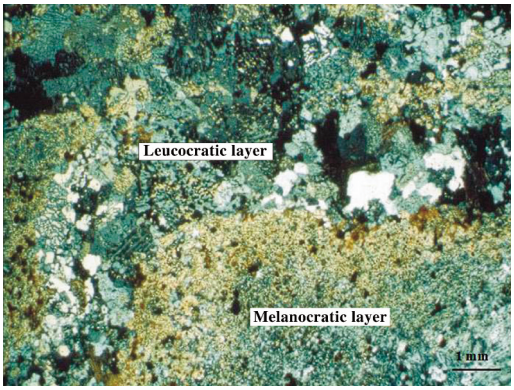

Figure 5. Injected migmatite. Leucocratic layers with medium grain size and melanocratic layers composed of fine grains. Large grain-sized leucocratic layers are mainly formed by mesopertitic K-feldspar, quartz, and minor amount of plagioclase, biotite, and magnetite. Fine grained melanocratic layers are mainly characterized by cordierite (often pinitised), plagioclase, decussated biotite, hercynite and corundum swarms and tourmaline. The boundaries of leucocratic layers are often characterized by biotite concentrations and the melanocratic layers are interlocked with lenticular medium-fine-grained domains formed by a quartz-feldspathic granoblastic texture.

The occurrence of graphic textures, euhedral plagioclase and biotite, and interstitial quartz indicate that also in IM the leucocratic layers are domains formed by a melt. However, the peculiar plagioclase texture suggests that the crystallization process in IM is different from that of M s.s. leucosome. Small plagioclase grains indicate that rapid growth from a melt has occurred and consequently the melt produced by metapelitic rocks has interacted with the quartz-diorite magma.

Hybrid rocks (HR)

These rocks are not foliated and are characterized by lenticular, plagioclase-bearing, quartz-diorite zones. In particular two main domains are clearly recognizable; the melanocratic domains, similar to the restitic layers in migmatites, and the heterogeneous domains in which quartz-diorite lenses and/or quartz-K-feldspar-rich portions (probably the leucosome remnants) are present.

In the restitic domains the presence of aggregated sub-millimeter sized orthopyroxene crystals is noteworthy. In these domains cordierite is the most abundant phase especially along the boundaries of restitic layers close to the quartz-diorite and shows a typical "cockade texture". The domains are characterized by the presence of sporadic sub-euhedral magmatic plagioclase almost totally replaced by clusters of cordierite. Hercynite + cordierite pseudomorphs have peculiar morphologies characterised by variable grade of hercynite concentration and shape. In particular, moving towards quartz-diorite, the hercynite concentration increases and the pseudomorphs assume a channel-shape. Ilmenite is also present in the restitic domains and often surrounded by biotite crowns. Restitic domains are often bordered by K-feldspar, biotite and ilmenite concentrations. Temperature reaches here the climax and we speculate that the thermal peak paragenesis is cordierite + plagioclase + hercynite + corundum + ilmenite + orthopyroxene ± rutile, strictly followed by tourmaline crystallization.

Restitic domains are mingled both with migmatitic leucosome and quartz-diorite domains. Moreover, leucosome and quartz-diorite grade into each other losing their typical features. In particular, the quartz in leucosome tends always to prevail over alkali feldspar especially moving towards the quartz-diorite contact. Quartz diorite domains show the following differences with respect to dark quartz-diorite rocks: 1) higher amounts of quartz; 2) thin K-feldspar crowns around plagioclase; 3) corroded phenocrysts of plagioclase, substituted by quartz; 4) no clinopyroxene; 5) higher amount of orthopyroxene; 6) centimetre-sized Fe-Ti oxides concentrations.

Analytical Methods

Thin sections were observed by a LEO FEG Scanning Electron Microscope (SEM) at the Bayerisches Geoinstitute, University of Bayreuth (Germany) equipped with a Back Scattered Electron (BSE) detector. Operating conditions were 20 KeV accelerating voltage, a working distance between 15 and 16 mm and a beam current of about 250 πA. The CSD of crystals is

a volumetric measure, but crystal sizes and numbers were measured from thin sections, which are two-dimensional slices. Therefore, the two-dimensional intersection data must be converted into three-dimensional CSD. This problem is not simple, except for spheres (see review on the subject of stereology in Royet, 1991). The approach and CSD Corrections program of Higgins (2000) was used to calculate the CSD. This is a modified Saltykov (1967) method, which 'unfolds' the intersection data to give the CSD. Most published CSD, including the early work of Higgins (1994), use an inappropriate conversion method (stereological techniques) and must be recalculated before they are compared with the data presented here. The CSD were plotted on a population density vs. size diagram following Marsh (1988), where the population density represents the number of crystals within a size range per unit volume divided by the width of that size range. Each bin is $10^{0.25}$ times the size of the previous bin because logarithmic length intervals were used. CSD diagrams are actually histograms, but are usually represented as x-y plots (Higgins, 2000). When examining such a graph it must be considered that the actual CSD falls to minus infinity [ln (0)] at either end. For small sizes this may be a real effect caused by a lack of small crystals, or an artefact produced by the technical limitations of recognizing small intersections in photographs. The latter can be excluded here, as all intersections were large enough to be measured. Lack of small grains is indicated on the CSD diagrams as an arrow pointing to ln (population density) = minus infinity: that is, no crystals in the interval.

Another important aspect is the significance of gaps in CSD meaning size bins with no crystals. The value of the population density on either side is not clear unless the histogram width is specified. This is particularly important for isolated bins. The size bins were chosen here to be sufficiently wide to exclude such gaps. It is always important to access the uncertainty in any parameter, albeit not easily measurable. The CSD correction program is an indirect distribution-method for stereological corrections of CSD determined from measurements of crystal outlines in thin section, outcrops etc. The procedure in the CSD correction program is described in Higgins (2000, 2002, 2006). Uncertainty in the corrections for contributions from larger size intervals is added. Errors are large for both small and large crystals. Points with error bars exceeding 1 ln unit were eliminated from the CSD used in this study. Error bars are omitted from the CSD diagrams for clarity. CSD can be represented by a straight line or broken segments that can be regressed. From the regression slope it is also possible to calculate the time of cooling by using the following equation:

$$\text{regression slope} = \exp^{(-1/Gt)} \qquad \text{Eq. 1}$$

where G is the crystal growth and t is time.

The cooling time data have been extrapolated using an average of the growth rate value ($2.8 * 10^{-8}$ $m*s^{-1}$) for plagioclase crystals as reported in several papers and calculated from Swanson (1977) experiments. It is worthwhile to notice

that the growth rate is generally not constant during the crystallization, so we have chosen a mean value. It is, then, important to underline that potential errors or uncertainties arise from the chosen growth rate concerning the cooling history of the magma.

The overall shapes of particular crystalline compounds are of interest because they are determined by the physico-chemical conditions of crystallization and the presence of neighbouring crystals (Sunagawa, 1987). Hence, determination of the crystal habit may reveal aspects of the crystallization environment. A crystal shape is needed also for the conversion of intersection lengths into CSDs (Higgins, 2000). The mean aspect ratios of the crystals (meaning for aspect ratio the three parameters short (S) intermediate (I) and long (L) dimensions (S:I:L)), were estimated from the statistical distribution of intersection width/length ratios (W/L), using the methods of Higgins (1994). For a massive rock, or one with a moderate fabric, as here, the mean W/L is equal to S/I (as reported in Higgins, 1994). The value of I/L is more difficult to determine precisely. Higgins (1994) suggested that I/L is approximately equal to skewness of the W/L distribution [(mean W/L–mode W/L)/standard deviation W/L]+0.5. However, for many rocks a better estimate can be made by comparing the volumetric phase proportion determined from the CSD with that measured from the total area of the phase (Higgins 2002). The inertia tensor method was used to determine the direction of the preferred orientation and the coherence of crystal orientations in the plane of the section (see description in Launeau and Cruden, 1998). This technique has the advantage that the contribution of each crystal to the total orientation ellipse is weighted for its elongation. The coherence of the crystal orientations was quantified by the ratio of the orientation ellipse axes: a sample with well-aligned crystals has an elongated orientation ellipse, and hence low values of the ratio of orientation ellipse axes (minor axis/major axis), whereas a sample without preferred orientation directions in the plane of interest will have circular orientation ellipse and, hence, an axial ratio of one.

It must be pointed out that the CSD analysis needs a large number of crystals to assess statistically representative results on distributions and shapes. Several images should be provided from several, replicated measurements in order to obtain realistic image analysis results. The CSD software by Higgins (2000) takes, in some way, into account preferred orientations in 3D (massive, lineated, foliated and no tailing fabric). For this reason, in the selected outcrop, 15 samples were cut from rock samples parallel and perpendicular to the exposed foliation, where present. The locations of the samples used for the CSD analysis cover approximately 2 km^2.

Results and discussion

Concerning the dark inner portion, based on the field collection, we plotted the samples from the farthest to the closest to the high-grade metamorphic rocks. Thus, we drew all the CSD diagrams together to compare them on the basis

of visual differences. Figure 6 shows a linear behaviour that might be interpreted as evidence of nucleation and growth of crystals in a crystal + melt system. Thus we can regard our system as a two-phase system (crystals + melt) that exhausts its chemical driving force (DeHoff, 1991). Despite the near equilibrium state of the two-phase system, the mixture is not in its lowest energy state (Voorhees, 1992). This means the occurrence of textural coarsening or Ostwald ripening process, in which the surface energy of aggregated small grains per unit volume is higher than that of aggregated large grains (Higgins, 1998; 2000; 2002). Therefore, in order to minimise the Gibbs free energy in the system, crystals smaller than a critical size will dissolve and "feed" the growth of larger crystals.. When a large crystal is surrounded by a small one, this latter will dissolve producing a local concentration of elements that will permit the large one to grow. On the other hand, if a large crystal is surrounded by another large crystal, this process will not occur. This is the reason why each crystal in the same rock has a different growth history reflected in its microchemical variation ("growth rate dispersion"). This interpretation is close to the above mentioned textural coarsening. Another possible explanation concerning plagioclase is based on the work of Lofgren (1974): crystal morphology changes with respect to undercooling degree. The calculated time of crystallization for this suite of rocks (dark quartz-diorite) ranges from ~1 kyr at the contact with

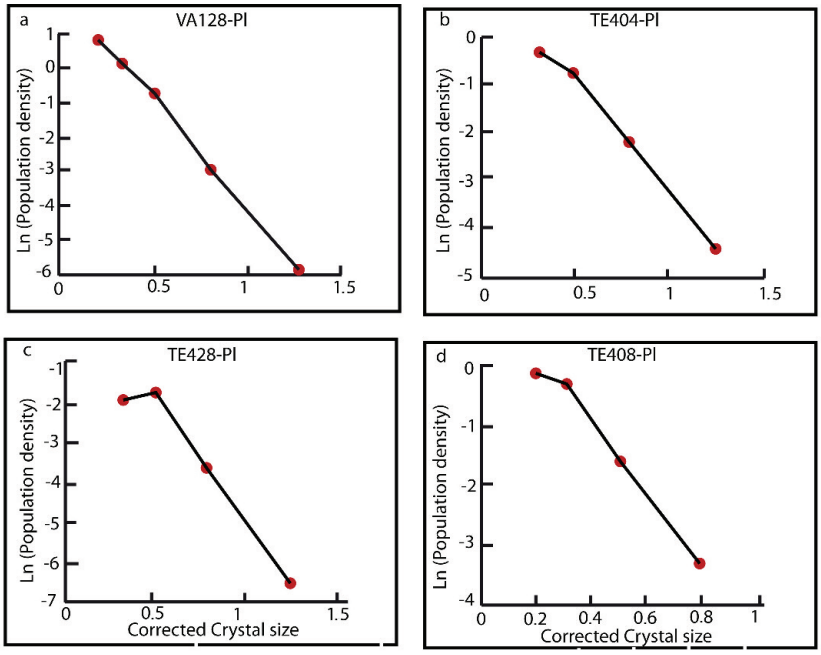

Figure 6. Crystal size distribution of plagioclase crystals in dark quartz-diorite. Around 0.5 mm there is a peak meaning the stop in crystallization processes and a growing of the formed crystals

wall rocks up to ~7 kyr for the light quartz-diorite samples, which is a quite reasonable time of cooling for a magmatic system. Crystallization time has been calculated using Eq. 1.

Concerning the plagioclase crystals of the light quartz-diorite, the interpretation on the CSD is quite different (Figure 6c). They all show an annealing process, underlined by the presence of a peak in the diagrams. Once nucleation ceases no new crystals form and the existing population may continue to grow to form a more even crystal size distribution (Marsh, 1988). At this point the small crystals underwent a grain boundary migration process (Means and Park, 1994) and resultantly, larger grains were formed. The final result is not a net change in crystal mass, but a Gaussian distribution of crystal sizes. Since most of the mass of the crystals lies in the intermediate size range (maximum value in the Ln of population density), the resulting CSD must show a maximum, skewed toward larger sizes. In general, grain boundary migration is a metamorphic process but it can also act in the magmatic stage, as shown by Hunter (1988). We can surmise that this process acted at subsolidus conditions after the nucleation stage. The cooling time calculated using Eq. 1 for these rocks from ~5 to ~8.5 kyr. However, a correct geometry of the light inner portion is difficult to establish and then to extrapolate to a correct cooling time, considering that some samples are closer to the metamorphic basement, while others are closer to the peraluminous body.

Moving towards the migmatites, Figure 7b and c shows a slight concavity upward of the curve after a negative slope. This trend possibly indicates that after nucleation there has been an accumulation of small grains which then started to dissolve in the residual melt. Given that this sample shows cordierite crystals (coming from the migmatite), an alternative interpretation would be that the smaller plagioclase crystals belong to the melanosome of migmatite, while the bigger ones belong to the quartz-diorite. Since Figure 7a shows the same trend as the one discussed above, it can be interpreted as a hybrid migmatite where the smaller plagioclase crystals are from migmatite while the bigger come from the quartz-diorite injections present in this rock. Finally, Figure 7a shows a concave upward trend which means accumulation of plagioclase crystals after their crystallization. The peak corresponding to the small grains is connected to plagioclase crystals belonging to the melanosome.

The behaviour of the migmatites and in particular the plagioclase in leucosomes is somehow different and complicated. Figures 8 shows a general flattening of the curve, while 8c shows a concave upward trend, that can be interpreted as an accumulation process in the system. This feature would suggest a melt loss during partial melting as reported also by Riedler et al. (2013): the effect is reflected in a virtual accumulation of big plagioclase crystals. The melt produced from the partial melting of metamorphic rocks escape to inject the quartz-diorite in contact with. Thus, the residual melt reflects accumulation of plagioclase crystals. Moreover, the presence of vermicular granophyric texture is interpreted as “dendrite segmentation” (Fowler et al., 2002; Means and Park, 1994), where dendritic refers to

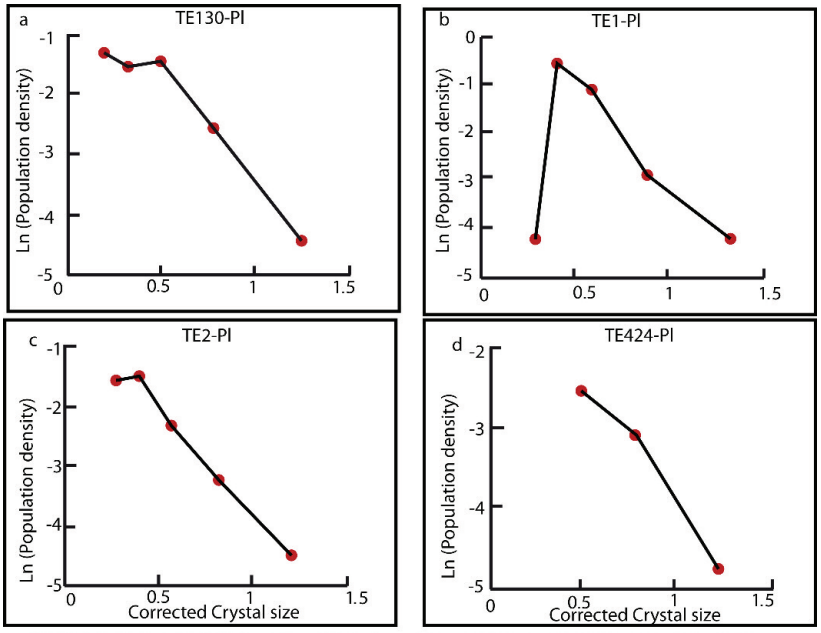

Figure 7. Crystal size distribution of plagioclase crystals in light quartz-diorite. Small concavity shown in the diagrams may indicate accumulation of small grains that afterwards dissolved in the melt.

habits characterised by geometries similar to the arrangement of bough on coniferous trees. This dendrite or granophyric texture is controlled by the crystallization rate and testifies a rapid cooling of a H_2O-saturated system. Indeed, the evaluated cooling period for this migmatite group is around 0.8 kyr, which fits well with the hypothesis of rapid cooling from a melt.

Figure 9 shows a concave upwards trend indicating a decrease in population density with increasing grain size. This could be explained by a textural coarsening as diffusion of elements proceeds. This means a normal crystallising process from a magmatic system. The cooling time for this group has been calculated to range from 0.4 up to 4 kyr in melt + solidus system. In general, CSD of injected migmatites are similar to those of magmatic rocks.

Figure 10a shows a bell-shaped curve followed by a straight trend of the curve. The bell-shaped curve represents the nucleation and growth of crystals and when the curve starts to be straight (mode of distribution) the nucleation and growth ceases and the coarsening starts. The small dimension of crystals can be referred to melanosome plagioclase crystals while the linear trend of the curve could be explained by crystallization from a melt without any removal of melt. Figure 10b shows evidence of an Ostwald ripening process, underlined by the presence of a change in the slope of the curve in the diagrams (around 0.5 mm). Once nucleation

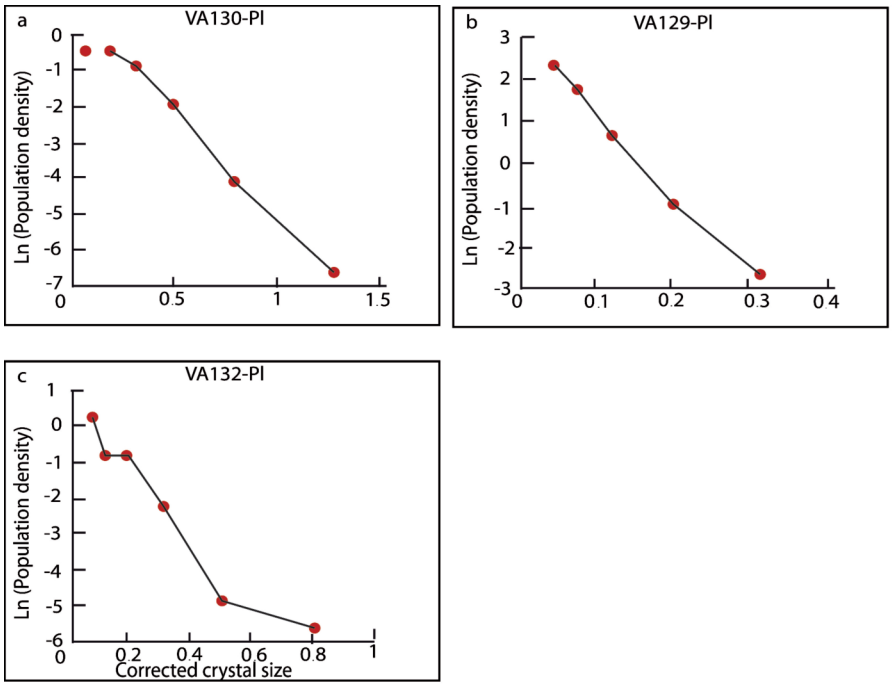

Figure 8. Crystal size distribution of plagioclase crystals in migmatites s.s.. We have measured crystal size distribution in leucosome of migmatite.

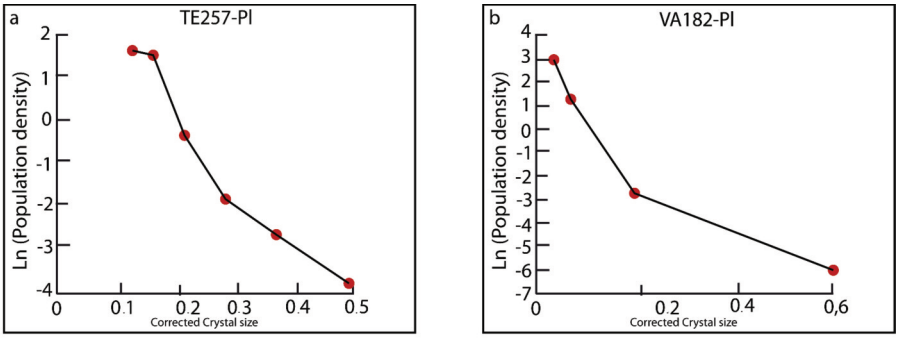

Figure 9. Crystal size distribution of plagioclase crystals in injected migmatites. The shape of the curves indicates a decrease in population density with increasing grain size.

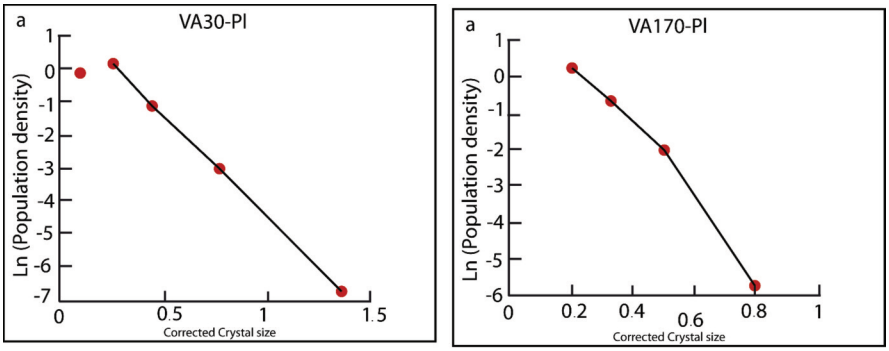

Figure 10. Crystal size distribution of plagioclase crystals in hybrid rocks.

ceases no new crystals will form and the existing population may continue to grow, to form a more even crystal size distribution.

Concluding remarks

The CSD diagrams for Gennargentu quartz-diorite samples show a variation which is form a linear trend, a slight bend, to a bell shape. This evolutionary trend could be explained as follows: dark quartz-diorite represents a magmatic system where the melt is always in contact with the forming crystals. Samples of the dark quartz-diorite, that reach the solidus in an average of time of ~5 kyr, show a bent curve which implies the formation of nuclei that are partly resorbed, such that the most numerous population of crystals does not reside in the small size but is shifted to around 200-300 μm. Finally, the presence of a strong bell-shaped curve in samples belonging to the light quartz-diorite testifies to a slow cooling (reaching the solidus in ~7.3 kyr) with a complete resorption of small nuclei and an increase of the average grain size.

Moving towards the contact with migmatites s.s. it is easy to notice a progressive bending of the curve which may indicate the presence of a bimodal distribution of crystals with a gap in the medium size range. Samples from Figure 6 are clearly magmatic, with the all grain sizes, while samples from figure 7 are hybrid because of the presence of melanosome enclaves and of quartz-diorite injections respectively. The smaller plagioclase crystals recorded during the measurements likely belong to the melanosome whereas the bigger crystals are clearly of magmatic origin.

Aknowledgment

This work was part of Valeria Misiti Ph.D. thesis and it was partially funded by Marie Curie phD training. The authors want to thank the two anonimous referees and the editor Michele Lustrino.

References

Armienti P., Francalanci L. and Landi P. (2007) - Textural effects of steady state behaviour of the Stromboli feeding system. *Journal of Volcanology and Geothermal Research*, 160, 86-98.

Armenante G. (1997) - Studio geopetrografico delle granodioriti peralluminose del Complesso Intrusivo del Gennargentu (Sardegna). Unpublished Msc Thesis, University of Rome La Sapienza.

Atzori P., Cirrincione R., Del Moro A. and Mazzoleni P. (2000) - Petrogenesis of late Hercynian calc-alkaline dykes of mid-eastern Sardinia: petrographical and geochemical data constraining hybridization process. *European Journal of Mineralogy*, 12, 1261-1282.

Berger A. and Roselle G. (2001) - Crystallization processes in migmatites. *American Mineralogist*, 86, 215-224.

Bindeman I.N. (2003) - Crystal size in evolving silicic magma chambers. *Geology*, 31, 367-370.

Brown M., Averkin Y.A., McLellan E.L. and Sawyer E.W. (1995) - Melt segregation in migmatites. *Journal of Geophysical Research: Solid Earth*, 100, 15655-15679,

Carmignani L., Barca S., Cappelli B., Di Pisa A., Gattiglio M., Oggiano G. and Pertusati P.C. (1992) - A tentative geodynamic model for the Hercynian basement of Sardinia. *IGCP n. 276*, Newsletter, 5, 61-82.

Carmignano L., Carosi R., Di Pisa A, Gattiglio M., Musumeci G., Oggiano D. and Pertusati P.C. (1994) - The Hercynian chain in SArdinia (Italy). *Geodinamica Acta,* 7, 31-47.

Carosi R., Gattiglio M., Musumeci G. and Oggiano G. (1992) - Geologia della catena ercinica in Sardegna. Zona a Falde. In: Geologia della catena ercinica in Sardegna. Guida all'escursione sul basamento Paleozoico della Sardegna, 77-108.

Carosi R., Montomoli C., Tiepolo M. and Frassi C. (2012) - Geochronological constraints on post-collisional shear zones in the Variscides of Sardinia (Italy). *Terra Nova*, 24, 42-51.

Casini L., Cuccuru S., Maino M., Oggiano G. and Tiepolo M. (2012) - Emplacement of the Arzachena Pluton (Corsica-Sardinia Batholith) and the geodynamics of incoming Pagaea. *Tectonophysics*, 544-545, 39-49.

Conte A.M., Perinelli C. and Trigila R. (2006) - Cooling kinetics experiments on different Stromboli lavas: Effects on crystal morphologies and phases composition. *Journal of Volcanology and Geothermal Research*, 155, 179-200.

Covey-Crump S.J. and Rutter E.H. (1989) - Thermally induced grain growth processes of calcite marbles on Naxos Island, Greece. *Contribution to Mineralogy and Petrology*, 101, 69-86.

Cozzupoli D., De Fazio P., Gaeta M. and Negretti G. (1994) - Lineamenti geopetrografici dei granitoidi peralluminosi del versante meridionale del Gennargentu, Sardegna (Nota 1). *Mineralogica et Petrografica Acta*, 37, 335-351.

Cozzupoli D., De Fazio P., Gaeta M., Massaro E.and Negretti G. (1995) - Le formazioni granitoidi del versante meridionale del Gennargentu, Sardegna (Nota II): lineamenti geopetrografici dei granitoidi monzonitici. *Mineralogica et Petrografica Acta* 38, 25-39.

Cozzupoli D., Gaeta M., Mastrobbatista P. and Negretti G. (1997) - Le formazioni granitoidi del Complesso Intrusivo del Gennargentu (Sardegna). Nota III: le metamorfiti di contatto. *Mineralogica et Petrografica Acta* 40, 27-44.

Dessau G., Duchi G., Moretti A. and Oggiano G. (1982) - Geologia della zone del valico di Correboi (Sardegna centro-orientale). Rilevamento, tettonica, giacimenti minerari (1). *Bollettino della Società Geologica Italiana*, 101, 497-522.

Franceschelli M., Gattiglio M., Pannuti F. and Fadda S. (1992) - Illite crystallinity in pelitic rocks from the External and Nappe zones of the Hercynian chain of Sardinia. *IGCP 276, Newsletter,* 5, 127-135.

Gaeta M., Mochi L., Invernizzi C., Conte A.M. and Misiti V. (2000) - Emplacement pressure conditions of Gennargentu Igneous Complex two mica granites, Central Sardinia, Italy. *Periodico di Mineralogia*, 69, 1-18.

Gaeta M., Giuliani A., Perilla S. and Misiti V. (2013) - Reddish metagranites from the Gennargentu Igneous Complex (Sardinia, Italy): insight into metasomatism induced by magma mingling. *Journal of Petrology,* 54, 839-859.

Garrido C.J., Kelemen P.B. and Hirth G. (2001) - Variation of cooling rate with depth in lower crust formed at an oceanic spreading ridge: plagioclase crystal size distributions in gabbros from the Oman

ophiolite. *Geochemistry, Geophysics, Geosystems*, 2, 136-162.

Higgins M.D. (1994) - Numerical modelling of crystal shapes in thin sections: Estimation of crystal habit and true size. *American Mineralogist*, 79, 113-119.

Higgins M.D. (1998) - Origin of anorthosite by textural coarsening: Quantitative measurements of a natural sequence of textural development. *Journal of Petrology*, 39, 1307-1323.

Higgins M.D. (1999) - Origin of megacrysts in granitoids by textural coarsening: a crystal size distribution (CSD) study of microcline in the Cathedral Peak granodiorite, Sierra Nevada, California. In: A. Castro, C. Fernandez, and J.L. Vigneresse, Eds., Uniderstanding granites: Integrative new and classical techniques, *Geological Society of London Special Publication,* 168, 207-219.

Higgins M.D. (2000) - Measurement of crystal size distribution. *American Mineralogist*, 85, 1105-1116.

Higgins M.D. (2002) - A crystal size-distribution of the Kiglapait layered intrusion, Labrador, Canada: evidence for textural coarsening. *Contributions to Mineralogy and Petrology*, 144, 314-330.

Launeau P. and Cruden A.R. (1998) - Magmatic fabric acquisition mechanisms in a syenite: results of a combined AMS and image analysis study. *Journal of Geophysical Research*, 103, 5067-5089.

Lowenstern J.B., Clynne M.A. and Bulle T.D. (1997) - Comagmatic A-type granophyre and rhyolite from Alid Volcanic Center, Eritrea, Northeast Africa. *Journal of Petrology*, 38, 1707-1721.

Marsh B.D. (1988) - Crystal size distribution (CSD) in rocks and the kinetics and dynamics of crystallization I. Theory. *Contributions to Mineralogy and Petrology*, 99, 277-291.

Marsh B.D. (1998) - On the interpretation of crystal size distributions in magmatic systems. *Journal of Petrology*, 39, 553-599.

Massaro E. (1995) - Rilevamento geopetrografico del settore compreso tra Punta la Marmora e la Valle del fiume Flumendosa. (Monti del Gennargentu, foglio n. 218, I NE-I NW). Unpublished Msc Thesis, University of Rome La Sapienza.

Misiti V. (2004) - Petrology of high-grade thermometamorphic rocks of Gennargentu (Sardinia, Italy). Unpublished Msc thesis, University of Rome La Sapienza.

Misiti V., Tecce F. and Gaeta M. (2005) - Fluids in low-pressure migmatites: a fluid inclusion study of rocks from the Gennargentu Igneous Complex (Sardinia, Italy). *Mineralogy and Petrology*, 85, 253-268.

Nam T.N., Otoh S. and Masuda T. (1999) - In-situ annealing experiments of octachloropropane as a rock analogue: kinetics and energetics of grain growth. *Tectonophysics*, 304, 57-70.

Padovano M., Dörr W., Elter F.M. and Gerdes A. (2014) - The East Variscan Shear zone: Geochronological constraints from the Capo Ferro area (NE Sardinia, Italy). *Lithos*, 196-197, 27-41.

Resmini R.G. (2007) - Modeling of crystal size distributions (CSDs) in sills. *Journal of Volcanology and Geothermal Research*, 161, 118-130.

Riedler C., White R.W. and Johnson T.E. (2013) - Migmatites in the Ivrea Zone(NW Italy): constraints on partial melting and melt loss in metasedimentary rocks from Val Strona di Omegna. *Lithos*, 175-176, 40-53.

Sunagawa I. (1987) - Surface microphotography of crystal faces. In: *Morphology of* crystalsPart A. Ed. By I. Sunagawa Reidel, Dordrecht, 321-365.

Zieg M.J. and Marsh B.D. (2002) - Crystal size distributions and scaling laws in the quantification of igneous textures. *Journal of Petrology*, 43, 85-101.

Submitted, June 2014 - Accepted, November 2014